J. Cell. Mol. Med. Vol 13, No 8A, 2009 pp. 1549–1564

Identification of pY19-caveolin-2 as a positive regulator of insulin-stimulated actin cytoskeleton-dependent mitogenesis

Hayeong Kwon, Kyuho Jeong, Yunbae Pak*

Department of Biochemistry, Division of Applied Life Science (BK21), Environmental Biotechnology National Core Research Center, Gyeongsang National University, Jinju, Korea

Received: January 11, 2008; Accepted: May 1, 2008

Abstract

Mitogenic regulation by caveolin-2 in response to insulin was investigated. Insulin triggered phosphorylation of caveolin-2 on tyrosine 19. Insulin increased the interaction between pY19-caveolin-2 and phospho-ERK, and that interaction was inhibited by a MEK inhibitor, U0126. Insulin-induced interaction of caveolin-2 with phospho-ERK was prevented when tyrosine 19 is mutated to alanine. Insulin re-localized phospho-ERK and pY19-caveolin-2 to the nucleus and their nuclear co-localization was impaired by U0126. Down-regulation of caveolin-2 by caveolin-2 siRNA arrested the insulin-induced nuclear localization of ERK with no change in the insulin-stimulated ERK activation. Of consequence, the caveolin-2 siRNA attenuated the ERK-mediated c-Jun and cyclinD1 expression and DNA synthesis by insulin. In addition, actin cytoskeleton influenced the nuclear translocation of caveolin-2-ERK complex. Collectively, our findings underscore the importance of pY19-caveolin-2 with the spatial coordination by insulin in ERK-mediated mitogenic regulation of insulin signalling and indicate that the phosphorylation of pY19-caveolin-2 is required for actin cytoskeleton-dependent ERK nuclear import.

Keywords: pY19-Caveolin-2 • ERK • insulin • caveolin-2 (Y19A) mutant • caveolin-2 siRNA • c-Jun • cyclinD1 • actin cytoskeleton

Introduction

Insulin transmits its signals through a cell surface tyrosine kinase receptor, which stimulates multiple intracellular signalling events. The insulin receptor (IR) undergoes activation upon insulin binding, leading to the generation of two major intracellular signalling pathways the phosphatidylinositol 3-kinase (PI3K)/Akt and the Ras/Raf/MEK/ERK: mitogen-activated protein kinase (MAPK) pathway [1, 2]. Insulin signalling in cellular mitogenesis *via* the MAPK pathway has been well established [3, 4]. Extracellular signal-regulated protein kinases (ERK) are activated when they are phosphorylated by MEK, which is activated by Raf [5]. In the MAPK signalling cascades, the ERK proteins are sites where diverse signals converge to elicit distinct biological responses through activation of the ERK effectors. When activated, ERK phosphorylates various downstream substrates involved in a multitude of cellular responses for mitogenesis [6–8]. Critical cellular processes such as proliferation, growth, differentiation, cytoskeletal remodelling, migration, cell cycle progression and apoptosis are known to be mediated by the MAPK pathway [9–11].

Upon mitogenic stimulation, ERK was re-localized from cytoplasm to nucleus [7, 12]. Comparison of the kinetics of ERK activation and nuclear translocation revealed that it is the active phosphorylated form of ERK that re-localizes into the nucleus [13]. Numerous transcription factors, including Elk-1, Egr-1, and c-Jun, are modulated by ERK in the nucleus for regulation of gene transcription [8–11, 14, 15]. The catalytically active ERK-mediated transcriptional events ultimately impinge on cell cycle elements, such as the induction of cyclinD1 for cell cycle progression [6–8]. In addition, cytoskeletal elements such as MAPs and Tau are also known to be regulated by ERK for cytoskeleton rearrangements affecting cellular morphology [16].

Caveolin, an integral membrane protein, is the primary protein component of caveolae membranes [17, 18]. The caveolin gene family consists of caveolin-1, -2 and -3. Caveolin-1 and -2 are expressed in most cell types, while caveolin-3 is expressed mainly in muscle cells [19]. Recent studies suggest that caveolins

*Correspondence to: Yunbae PAK, Ph.D.
Department of Biochemistry, Gyeongsang National University,
Jinju 660-701, Korea.
Tel.: 82-55-751-5961
Fax: 82-55-759-9363
E-mail: ybpak@nongae.gsnu.ac.kr

doi:10.1111/j.1582-4934.2008.00391.x

function as scaffolding proteins to interact with signalling molecules like G-proteins, receptor tyrosine kinases (RTKs), Src-like kinases, eNOS, Ras and ERK [17, 18]. Thus, caveolins are known to play an active role in a variety of cellular processes [20, 21]. Despite numerous findings of caveolin regulation in signalling, most of the studies reported have concentrated exclusively on the role of caveolin-1. Of interest, the MAPK-mediated signal cascade is negatively regulated by the relative abundance of caveolin-1 [22–27]. The expression of caveolin-1 is significantly reduced in human breast cancer cells [22, 23]. The cyclin D1 gene is inhibited during overexpression of caveolin-1 [24]. The loss of mitogenic signalling in senescent cells is related to their up-regulation of caveolin-1 [27–29]. Caveolin-1, thus, affects the regulatory mechanism of cell growth negatively and reduces not only cell growth but also tumourigenecity.

Caveolin-2, which is 38% identical and 58% similar to caveolin-1 is widely presented in many cell types [19, 30] and has been known generally for its structural role in caveolae formation [17–21]. Primary sequence analysis of caveolin-2 reveals that caveolin-2 contains a putative tyrosine kinase recognition motif (QLFMADDSpY) at tyrosine 19 and a conserved SH2 domain-binding motif (pYADP) at tyrosine 27 [31, 32]. Although recent reports show that caveolin-2 can be phosphorylated on tyrosine 19 and 27 by c-Src [31, 32] and serine-phosphorylated on 23 and 36, likely through the action of casein kinase 2 [33], and that caveolin-2 deficient transgenic mice have pulmonary dysfunction [34], there have been no data demonstrating that caveolin-2, per se, can modulate signalling in a manner similar to caveolin-1. Thus, the exact physiological role of caveolin-2 remains unknown. Therefore, except for its structural role in the formation of caveolae, little is known concerning any role of caveolin-2, especially in the regulation of cell mitogenesis. In our previous study, we showed that caveolin-2 enhances the insulin-induced cell cycle in Hirc-B fibroblasts [35]. Induction of the caveolin-2 gene was up-regulated in response to insulin and the endogenous caveolin-2 enhanced the G1 to S phase transition of cell cycle whereas caveolin-1 inhibits when cells were expressed with recombinant caveolin-1. However, the molecular mechanisms by which caveolin-2 regulates cell proliferation have not been established.

Accordingly, the present study was conducted to assess the molecular mechanism of the positive modulatory role of caveolin-2 in the regulation of the MAPK-mediated insulin mitogenic signalling. Here, we provide evidence that pY19-caveolin-2 physically associates with phospho-ERK and the complex co-localizes in the nucleus in response to insulin. pY19-Caveolin-2 is required for ERK translocation, gene transcription, cell proliferation and cell cycle progression *via* the insulin-induced MAPK signalling pathway. In addition, nuclear translocation of the caveolin-2-ERK complex depends on an intact actin cytoskeleton. These findings suggest that pY19-caveolin-2 is an important key mediator for ERK translocation and is required for actin cytoskeleton-dependent MAPK-mediated mitogenesis by insulin.

Materials and methods

Cell culture and treatment

Rat1 and 3T3L1 fibroblasts and H9c2 cardiomyoblasts were grown in Dulbecco's modified Eagle's medium (DMEM: Gibco/BRL) containing 5 mM D-glucose supplemented with 10% (v/v) FBS and 0.5% penicillin/streptomycin (Sigma Chemical Co, St Louis, MO, USA) in a 5% CO_2 incubator at 37°C. Human insulin receptor-overexpressed rat 1 fibroblast (Hirc-B) cells were grown in DMEM containing 5 mM D-glucose supplemented with 10% (v/v) fetal bovine serum (FBS) (Cambrex Bio Science), 100 nM methotrexate (Sigma-Aldrich Chemie GmbH, Steinheim, Germany) and 0.5% gentamycin (Gibco) in a 5% CO_2 incubator at 37°C as previously described [35]. Cells were serum starved in serum-free DMEM containing 0.2% BSA for 4 or 18 hrs as indicated. Cells were then pretreated with or without 10 μM U0126 (#9903, Cell Signaling) for 2 hrs, 100 nM wortmannin (W1628, Sigma) for 1 hr, 1 μM cytochalasin-D (CCD: C8273, Sigma) for 15 min., or 1 μM latrunculin B (LatB: 428020, Calbiochem) for 30 min. followed by stimulation with or without 100 nM insulin (Human insulin, Novo Nordisk) for 10 min. or 3 hrs.

SDS-PAGE and immunoblot analysis

For the protein extraction, cells were washed twice with ice-cold phosphate-buffered saline (PBS) and lysed with RIPA buffer (50 mM HEPES, 150 mM NaCl, 100 mM Tris-HCl (pH 8.0), 0.25% deoxycholic acid, 0.1% SDS, 5 mM EDTA, 10 mM NaF, 5 mM DTT, 1 mM phenylmethylsulfonyl fluoride (PMSF), 1 mM sodium ortho-vanadate, 20 μM leupeptin and 100 μM aprotinin). The lysate was put on ice for 30 min. and microcentrifuged at 12,000 rpm for 20 min. at 4°C. Aliquots from the clear supernatant were taken for protein quantification as determined by the Bradford assay (Bio Rad). Equal amounts of samples (50 μg) were separated on 10 or 12.5% (w/v) SDS-polyacrylamide gels and transferred to polyvinylidene difluoride (PVDF) membrane (Millipore). Transfers were blocked overnight at 4°C with 5% (v/v) nonfat dry milk in TBS, 0.1% (v/v) Tween 20 and then incubated for 2 hrs at room temperature (RT) in the primary antibody. The primary antibodies used were as follows: caveolin-2 (BD 610685; diluted 1/250), phosphotyrosine-PY20 (BD 610000; 1/500), ERK1 (BD 610031; 1/2500), ku-70 (BD 611892; 1/500) and c-Jun (BD 554083; 1/500) antibodies from BD Transduction Laboratories; F-actin (sc-1616; 1/200), α-tubulin (sc-5286; 1/200), and IRβ (sc-711; 1/200) antibodies from Santa Cruz Biotechnology; phospho-ERK (Thr202 and Tyr204) (#9101; 1/1000), and p44/42 MAPK (#9102; 1/1000) antibodies from Cell Signaling; pY19-caveolin-2 (ab3417; 1/500) antibody from Abcam; cyclinD1 (AB1320; 1/500) antibody from Chemicon. The membranes were washed with TBS, 0.1% (v/v) Tween 20 and incubated for 1 hr at RT in horseradish peroxidase-conjugated anti-rabbit (#W4011) or anti-mouse (#W4021) secondary antibodies (Promega; 1/15000) in 5% (v/v) nonfat dry milk in TBS, 0.1% (v/v) Tween 20. The immunoblots were developed using the ECL detection reagent (RPN2106, Amersham Biosciences).

Immunoprecipitation

Serum-starved cells were incubated with or without 100 nM insulin for 10 min. after being preincubated with or without 10 μM U0126 for 2 hrs or 100 nM wortmannin for 1 hr, washed with ice-cold PBS, and lysed in buffer

A (1% Triton X-100, 150 mM NaCl, 10 mM Tris-HCl (pH 7.4), 1 mM EDTA, 1 mM EGTA (pH 8.0), 0.2 mM sodium ortho-vanadate, 0.2 mM PMSF, 0.5% Nonidet P-40 (Igepal CA-630, octyl phenoxylpolyethoxylethanol, 198596: ICN Biomedicals) [36, 37]. The cell lysates were centrifuged at 12,000 rpm for 20 min. at 4°C and the supernatants were subjected to immunoprecipitation with either anti-caveolin-2, anti-ERK, anti-phospho-ERK, anti-IRβ, or anti-PI3K antibodies. Lysates were rotated overnight at 4°C, then 30 μl of protein G plus Agarose (IP04: Calbiochem) was added and the mixture was rotated for 4 hrs at 4°C. The immunocomplexes were collected by centrifugation at 12,000 rpm for 10 min. at 4°C and washed three times with ice-cold lysis buffer. After the final wash the pellet was resuspended in 30 μl of 2X SDS-PAGE sample buffer. Immunoprecipitated samples were then resolved, separated by SDS-PAGE and subjected to immunoblot analyses using the specific antibodies against proteins of interest.

Because of its property to solubilize caveolins bound to cholesterol-rich membrane domains, buffer B (buffer A containing 60 mM n-octylglucoside (OG, 494460: Calbiochem)) was employed to analyse caveolin-2 and ERK interaction. Cells incubated with or without 100 nM insulin for 10 min. after being preincubated with 10 μM U0126 for 2 hrs and cells transiently co-transfected with wild type caveolin-2 (WT) or site-directed Y19A caveolin-2 mutant (Y19A) were lysed in buffer B and processed for immunoprecipitation as described above.

Transient expression of mutant caveolin-2 (Y19A)

A full-length caveolin-2 cDNA (NCBI research; Rattus norvegicus, NM131914) was subcloned into pcDNA3 vector using *Eco*RI - *Xho* I (NEW ENGLAND BioLabs). A construct encoding caveolin-2 (Y19A) was generated by PCR mutagenesis using mutated oligonucleotides. These vectors (pcDNA3 alone, pcDNA3 + caveolin-2 (WT) and pcDNA3 + caveolin-2 (Y19A)) were transiently transfected into cells using the Lipofectamin LTX transfection reagent (Invitrogen) as per the manufacturer's instructions. Thirty-six hours after transfection, cells were scraped into boiling sample buffer. Recombinant expression was confirmed by SDS-PAGE/immuno-blotting and caveolin-2 and ERK interaction was analysed by immunoprecipitation.

Silencing of caveolin-2 gene by siRNA

The small interfering RNAs (siRNAs) were designed to target the following sequences: scramble control; 5′-GGAAAGACUGUUCCAAAAA-3′, caveolin-2 siRNA duplexes; sense (GUAAAGACCUGCCUAAUGGUU) and antisense (5′-PCCAUUAGGCAGGUCUUUACUU). The siRNA duplexes were synthesized and purified by Dharmacon Research, Inc. Transfection of siRNA duplexes was carried out using DhamaFECT Transfection Reagents (Dharmacon) for 48 hrs. The transfected cells were serum starved for 4 hrs and pretreated with or without U0126 (10 μM) for 2 hrs followed by stimulation with or without 100 nM insulin for 10 min. or 3 hrs. Cells were then subjected to immunoblot analysis and processed for immunostaining as described below.

Immunofluorescence microscopy and quantitative detection of fluorescence staining

Effects of insulin and caveolin-2 down-regulation by caveolin-2 siRNA on cellular translocation of caveolin-2, pY19-caveolin-2, and ERK were investigated by immunofluorescence microscopy. Briefly, cells were transfected either by scramble or caveolin-2 siRNAs for 48 hrs after plating on coverslips. Transfected cells were serum-starved for 4 hrs in DMEM containing 0.2% BSA. Cells, after being preincubated with or without 10 μM U0126 for 2 hrs, 100 nM wortmannin for 1 hr, 1 μM CCD for 15 min., or 1 μM LatB for 30 min., were then incubated with 100 nM insulin for 10 min., washed twice with ice-cold PBS, and fixed with 3.7% paraformaldehyde in PBS for 20 min. at RT. The fixed cells were rinsed with PBS and incubated with 0.1% Triton X-100 in PBS for 30 min. Permeabilized cells were rinsed with PBS, incubated with 1% BSA in PBS for 30 min. and then with anti-caveolin-2, anti-ERK, anti-phospho-ERK and anti-pY19-caveolin-2 antibodies diluted 1/200 in 1% BSA in PBS for 2 hrs at RT. After washing three times with PBS, the primary antibodies were detected with TRITC-conjugated anti-mouse (1/100 dilution), FITC-conjugated anti-rabbit (1/100 dilution), and Alexa Fluor® 488-conjugated anti-mouse (1/250 dilution) IgG antibody (Invitrogen) TRITC-conjugated anti-rabbit (1/100 dilution) IgG antibodies (Sigma) for caveolin-2, ERK, phospho-ERK or pY19-caveolin-2. To localize actin filaments, cells were incubated with FITC-conjugated phalloidin (P5282: Sigma) for 2 hrs at RT. Nuclei were fluorescently labelled with 4', 6-diamidino-2-phenylinodole (DAPI) (D8417: Sigma) for 15 min. at RT. The coverslips were then washed and mounted on glass slides. Fluorescent images were obtained using appropriate filters on an Olympus BX51 microscope and imaged with an Olympus DP-71 digital camera with an image processing system equipped with Image-ProPlus 6.1 (MediaCybernetics). Neither labelling in the absence of the primary antibody nor cross-reactivity between secondary and primary antibodies was observed.

Fluorescence staining was quantified by image analysis performed using ImageJ software [38, 39]. Quantitative fluorescence data were exported from ImageJ generated histograms into Microsoft Excel software for further analysis. Averages and standard errors were computed over 3 or 5 images per condition for a minimum of 150 cells per condition. The DAPI staining mask was used to define the nuclear region of interest (ROI). Measurement of nuclear co-localization of caveolin-2 with ERK or pY19-caveolin-2 with phospho-ERK was performed using the Colocalization Finder Plugin from ImageJ, which allowed us to highlight and select the caveolin-2/ERK or pY19-caveolin-2/phospho-ERK with a specified ratio of intensities measured in the merge mask from both caveolin-2 and ERK or pY19-caveolin-2 and phospho-ERK masks. Using the Image Calculator from ImageJ, the DAPI mask was subtracted from the merge mask to create a staining mask defining the cytoplasmic ROI. Nuclear translocation was determined with binary image masks, which were created of either ERK or pY19-caveolin-2, and DAPI positive staining to define ROI for analysis. The DAPI mask was subtracted from the ERK or pY19-caveolin-2 mask to create a staining mask defining the cytoplasmic ROI using the Image Calculator from ImageJ. Nuclear and cytoplasmic staining intensities were compared to give the nuclear:cytoplasmic ratio.

Nuclear fractionation

Nuclear and cytosol lysates were prepared following the recommendation of the manufacturer of the Nuclear Extraction Kit (Chemicon International, Cat. No.2900). Briefly, cells were incubated with or without 100 nM insulin for 10 min. after being preincubated with or without 10 μM U0126, 100 nM wortmannin for 1 hr, 1 μM CCD for 15 min., or 1 μM LatB for 30 min. washed with ice-cold PBS, and centrifuged at 250 × *g* for 5 min. at 4°C. The pellet was suspended in Cytoplasmic Lysis Buffer and recentrifuged at 8000 × *g* for 20 min. at 4°C. The supernatants were collected as cytoplasmic extracts. The nuclear pellets were resuspended in Nuclear Extraction Buffer and debris was removed by centrifugation at 16,000 × *g* for 5 min. at 4°C. The supernatants were finally collected as nuclear extracts and processed for immunoblot analysis as described above.

Cell proliferation assay

The 5-bromo-2-deoxy-uridine (BrdU: B5002, Sigma) labelling was performed to examine cell proliferation by measuring DNA replication in insulin-treated Hirc-B cells with or without caveolin-2 siRNA transfection. Transfected cells were preincubated with or without 10 μM U0126 for 2 hrs, treated with or without 100 nM insulin for 10 min., and then incubated for 16 hrs in the presence of BrdU. After 16 hrs incubation, cells were fixed with 3.7% formaldehyde for 10 min. at RT and permeabilized with 0.3% Triton X-100. The fixed cells were incubated with 50 μl of anti-BrdU antibody (NA20: Oncogene) at 37°C for 1 hr. After repeated washing with PBS, cells were incubated with 50 μl of TRITC-conjugated anti-mouse antibody (diluted in PBS; 1/100) at 37°C for 1 hr. BrdU incorporation into DNA was assessed by measuring the absorbance at 543 nm wavelength using immunofluorescence microscopy.

RT-PCR analysis

Total RNA was extracted with TRIzol reagent (SolGent Co., Ltd.) according to the manufacturer's instructions. cDNA was generated using a reverse transcription kit (Accupower RT PreMix, Bioneer). The cDNA was used as the template for the subsequent PCR amplification. PCR primers for glyceraldehyde-3-phosphate dehydrogenase (GAPDH): 5′-ACCACCATGGAGAAGGCTGG-3′ and 5′-CTCAGTGTAGCCCAGGATGCC-3′; CyclinD1: 5′-CTGAGGAGACCTGCGCGC-3′ and 5′-TCGATGTTCTGCTGGGCCT-3′; p21: 5′-ATGTCCGATCCTGGTGATGTCC-3′ and 5′-TCAGGGCTTTCTTGCAGAAGA-3′. PCR was performed using AccuPower PCR PreMix (Bioneer) kit with a 2-min. initial denaturation at 95°C and 20~30 cycles of 30 sec. at 95°C, 30 sec. at 50°C and 1 min. at 72°C; these cycles were followed by a 5-min. extension at 72°C. The PCR fragments were separated by running on 1% agarose gels.

Densitometry analysis

Chemiluminescent images of immunoblots were analysed by scanning densitometry using Kodak Gel Logic 100 Imaging System (Eastman Kodak Co.). Multiple exposure of each blot was used to obtain gray-scale images of each chemiluminescent band. Bands were visualized on a UV transilluminator and photographed

Statistical analysis

Data are expressed as mean ± S.E. An unpaired Student's t-test was used to compare treatment groups with significance established at a level of $P < 0.05$.

Results

Insulin induces tyrosine phosphorylaion of caveolin-2

To investigate the phosphorylation of caveolin-2 and its functional significance in response to insulin, cells were treated with insulin for a detailed time-course experiment and insulin-induced tyrosine phosphorylation of caveolin-2 was characterized (Fig. 1). Insulin triggered caveolin-2 tyrosine phosphorylation as early as 10 min. after insulin incubation. Phosphotyrosine-caveolin-2 was reached maximum 2.1-fold increase at 60 min. and gradually returned to 1.3-fold at 180 min. In contrast, pY19-caveolin-2 was increased 1.3-fold starting at 10 min., reached maximal level of 1.6-fold at 60 min. and sustained the level throughout until 180 min.

Insulin increases the association of phosphotyrosine-caveolin-2 with the insulin receptor

To investigate how tyrosine phosphorylation of caveolin-2 influences in insulin signalling, we first examined the association between IR and caveolin-2 (Fig. 2). During an insulin time course, the interaction of IR with caveolin-2 was increased to the maximum 4-fold at 10 min. (Fig. 2A). When the interaction with phosphotyrosine-caveolin-2 was examined, 5.4-, 6.9- and 2.9-fold increases at 10, 60 and 180 min., respectively, was observed (Fig. 2B). In contrast, the IR interaction with pY19-caveolin-2 showed no detectable changes in response to insulin (Fig. 2C). These results show that pY19-caveolin-2 does not involve in upstream insulin signalling through direct interaction with IR. However, the results suggest that pY27-caveolin-2, another phosphotyrosine-caveolin-2, might be involved in the insulin signalling.

Insulin triggers association between pY19-caveolin-2 and phospho-ERK

We have investigated insulin-induced tyrosine phosphorylation of caveolin-2 and its interaction with phospho-ERK by immunoprecipitation analyses after cells were treated with U0126. U0126 completely abolished insulin-induced interaction of caveolin-2 with phospho-ERK (Fig. 3A). When the insulin-induced tyrosine phosphorylation of caveolin-2 was analysed, pY19-caveolin-2 was 2-fold increased but U0126 suppressed the phosphorylation to basal level. The interaction of ERK with pY19-caveolin-2 was increased 2-fold by insulin but decreased below the basal level by U0126 (Fig. 3B). Of interest, the basal interaction of phospho-ERK with pY19-caveolin-2 was increased by insulin (Fig. 3C). These data suggest that insulin promotes phosphorylation of caveolin-2 on tyrosine 19 and ERK in the caveolin-2-ERK complex. When the effect of wortmannin on the insulin-induced caveolin-2 interaction with ERK was examined, the interaction of caveolin-2 with phospho-ERK and phosphorylation of pY19-caveolin-2 showed no significant changes (Fig. 3D). Furthermore, the insulin-elicited interaction of ERK with pY19-caveolin-2 was also not changed (Fig. 3E). Thus, our data demonstrate that insulin-induced phosphorylation of caveolin-2 at tyrosine 19 and its interaction with ERK was mediated independently of the PI3K signalling pathway.

In order to verify physiological relevance of the interaction between caveolin-2 and phospho-ERK, we further examined the

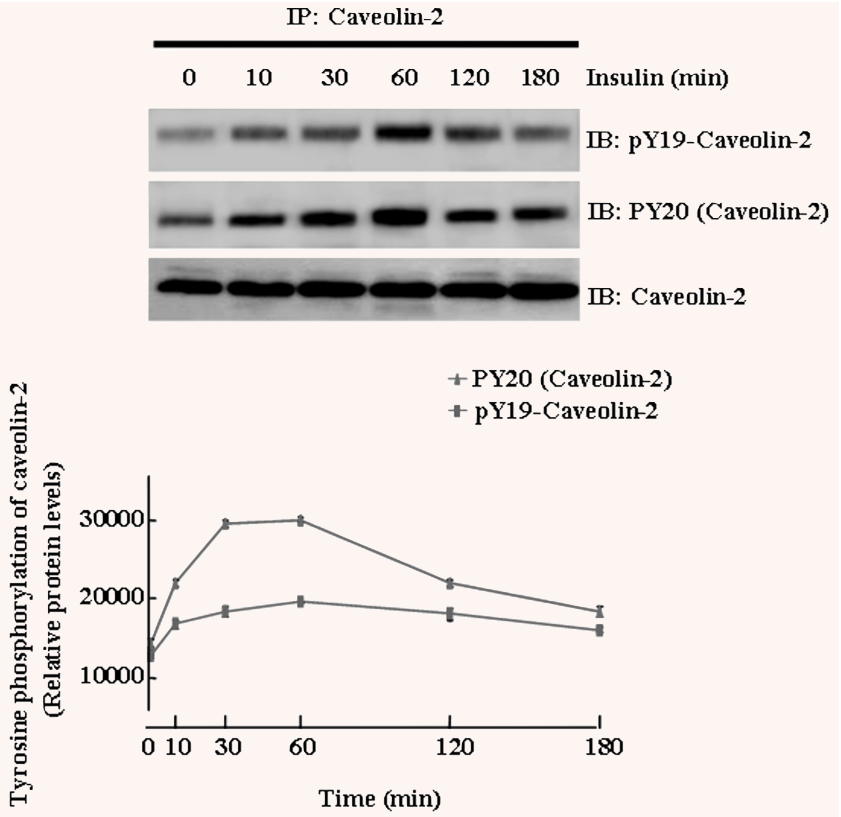

Fig. 1 Insulin-induced tyrosine phosphorylation of caveolin-2. After serum starvation, Hirc-B cells were treated with 100 nM insulin for different time periods. The whole cell lysates (WCL) were immunoprecipitated with anti-caveolin-2 antibody and subjected to immunoblot analysis with anti-pY19-caveolin-2 and anti-phosphotyrosine PY20 antibodies. Tyrosine phosphorylation of caveolin-2 levels were quantified by densitometry. The results represent mean ± S.E. of indicated independent experiments, PY20 (caveolin-2) ($n = 4$), pY19-caveolin-2 ($n = 3$).

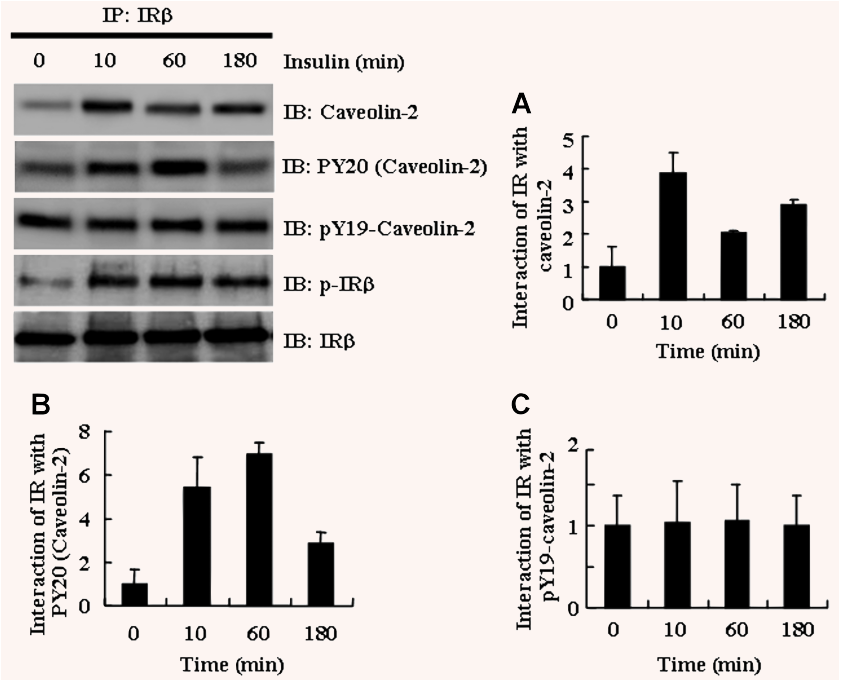

Fig. 2 Insulin-induced association between phosphotyrosine-caveolin-2 and insulin receptor. Hirc-B cells were incubated with 100 nM insulin in a time course as indicated. WCL were immunoprecipitated with anti-IRβ antibody and subjected to immunoblot analysis with anti-pY19-caveolin-2, anti-phosphotyrosine PY20 and anti-IRβ antibodies as indicated. Insulin receptor (IR) interaction with caveolin-2; (**A**) PY20 (caveolin-2); (**B**) and pY19-caveolin-2; (**C**) was quantified by densitometry. The results represent mean ± S.E. of three independent experiments.

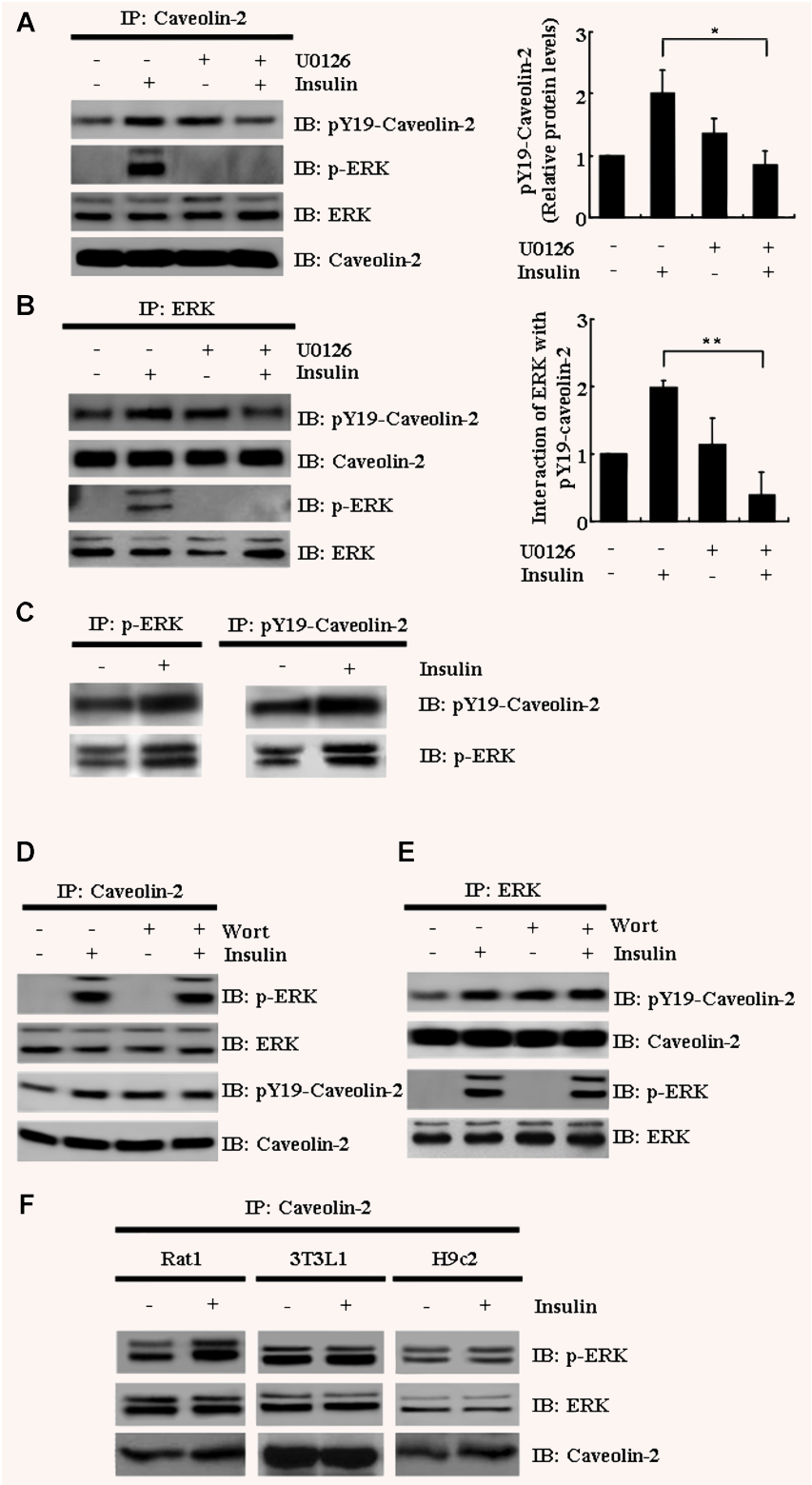

Fig. 3 Effects of U0126 and wortmannin on the insulin-induced association between phosphotyrosine-caveolin-2 and phospho-ERK. (**A**) Hirc-B cells were treated with or without 10 μM U0126 for 2 hrs before100 nM insulin treatment for 10 min. WCL were immunoprecipitated with anti-caveolin-2 antibody and subjected to immunoblot analysis with anti-ERK, anti-phospho-ERK, anti-caveolin-2 and anti-pY19-caveolin-2 antibodies as indicated. pY19-Caveolin-2 protein levels were quantified by densitometry. Quantification shown was the relative levels of pY19-caveolin-2 detected as compared to the control samples; mean ± S.E., $n = 3$. *, $P < 0.01$; phosphorylation levels differed significantly compared with insulin-stimulated samples. (**B**) Equal amounts of WCL were immunoprecipitated with anti-ERK antibody and subjected to immunoblot analysis with anti-pY19-caveolin-2, anti-caveolin-2, anti-ERK and anti-phospho-ERK antibodies as indicated. pY19-Caveolin-2 protein levels were quantified by densitometry. Quantification represents the relative intensity to the control cells; mean ± S.E., $n = 4$. **, $P < 0.001$; phosphorylation levels differed significantly compared with insulin-stimulated samples. (**C**) Equal amounts of WCL were immunoprecipitated with anti-phospho-ERK and anti-pY19-caveolin-2 antibodies and subjected to immunoblot analysis with anti-pY19-caveolin-2 and anti-phospho-ERK antibodies as indicated. (**D**) Cells were treated with or without 100 nM wortmannin for 1 hr before 100 nM insulin treatment for 10 min. WCL were immunoprecipitated with anti-caveolin-2 antibody and subjected to immunoblot analysis with anti-ERK, anti-phospho-ERK, anti-caveolin-2 and anti-pY19-caveolin-2 antibodies as indicated. (**E**) Equal amounts of WCL were immunoprecipitated with anti-ERK antibody and subjected to immunoblot analysis with anti-pY19-caveolin-2, anti-caveolin-2, anti-ERK and anti-phospho-ERK antibodies as indicated. (**F**) Rat1 and 3T3L1 fibroblasts and H9c2 cardiomyoblasts were treated with or without 100 nM insulin for 10 min. WCL were immunoprecipitated with anti-caveolin-2 antibody and subjected to immunoblot analysis with anti-phospho-ERK, anti-ERK and anti-caveolin-2 antibodies as indicated.

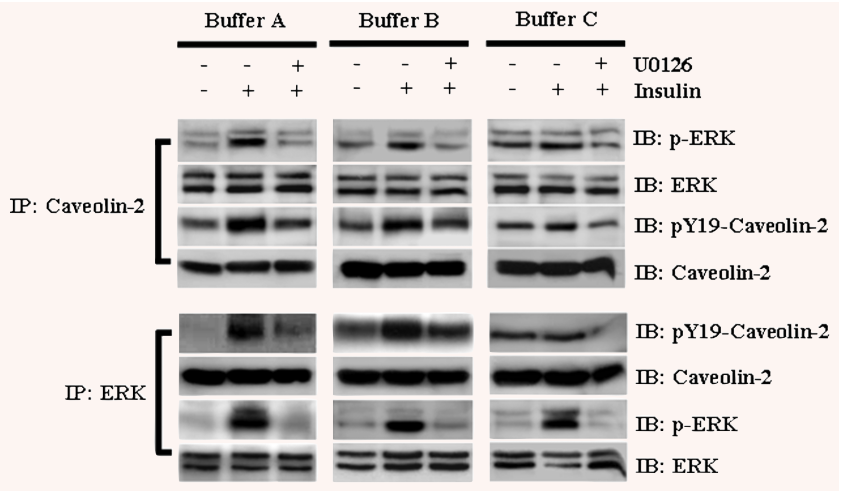

Fig. 4 Effect of nonionic, non-denaturing detergents on the caveolin-2 solubilization and interaction between caveolin-2 and ERK. Hirc-B cells were treated with 10 μM U0126 for 2 hrs before100 nM insulin treatment for 10 min. Cells were then lysed in either 1% Triton X-100 lysis buffer containing 0.5% Nonidet P-40 alone **(buffer A)**, 1% Triton X-100 lysis buffer containing 0.5% Nonidet P-40 + 60 mM OG **(buffer B)**, or 1% Triton X-100 lysis buffer containing 60 mM OG alone **(buffer C)** as described under 'Materials and Methods'. WCL were immunoprecipitated with anti-caveolin-2 and anti-ERK antibodies and subjected to immunoblot analysis with anti-phospho-ERK, anti-ERK, anti-pY19-caveolin-2 and anti-caveolin-2 antibodies as indicated.

interaction in Rat1 and 3T3L1 fibroblast cells, and H9c2 cardiomyoblast cells derived from embryonic rat heart tissue. The interaction of caveolin-2 with phospho-ERK was confirmed in the various cell types and increased by insulin in Rat1 fibroblast cells (Fig. 3F).

Nonidet P-40 and n-octylglucoside solubilize caveolin-2 while retaining caveolin-2-ERK interaction

Caveolin-2 is mostly bound to cholesterol-rich membrane domains. Since Triton X-100 has been reported to solubilize the membrane domains inefficiently, we tested additional detergents, Nonidet P-40 for solubilizing membrane proteins during isolation of membrane-protein complexes and OG for disrupting cholesterol-rich domains to promote greater solubilization during cell lysis for co-immunoprecipitation analysis between caveolin-2 and ERK. When caveolin-2 and ERK were immunoprecipitated in lysis buffer B (1% Triton X-100 lysis buffer containing 0.5% Nonidet P-40 + 60 mM OG), insulin-stimulated interaction of both caveolin-2 with phospho-ERK and ERK with pY19-caveolin-2, respectively, showed almost same results obtained from samples immunoprecipitated in lysis buffer A (1% Triton X-100 lysis buffer containing 0.5% Nonidet P-40 alone) or C (1% Triton X-100 lysis buffer containing 60 mM OG alone) (Fig. 4). Buffer B and C solubilized more caveolin-2 than buffer A. However, the insulin-induced interaction between caveolin-2 and ERK was more evident in buffer B than C. Thus, it appears that both Nonidet P-40 and OG are required for optimal caveolin-2 solubilization and isolation of caveolin-2-ERK complex without altering the binding affinity of those two proteins.

Tyrosine 19 is essential for interaction with phospho-ERK and activation of ERK

To verify the association between pY19-caveolin-2 and phospho-ERK following insulin stimulation is caveolin-2 phosphorylation at tyrosine 19 specific, we mutated caveolin-2 tyrosine 19 to alanine (Y19A). Figure 5 shows that the caveolin-2 (Y19A) mutant is no longer phosphorylated at tyrosine 19 and the insulin-stimulated caveolin-2 interaction with phospho-ERK is completely abolished. The reverse immunoprecipitation experiment with ERK confirmed the decreased interaction with pY19-caveolin-2. Of interest, Y19A mutant cells exhibited the inhibition of insulin-induced ERK activation. Thus, our data demonstrate that the phosphorylation of caveolin-2-bound ERK requires phosphorylation of caveolin-2 on tyrosine 19.

Insulin promotes nuclear co-localization of pY19-caveolin-2 and phospho-ERK

ERK activation is characterized by its nuclear translocation [7, 12, 13]. Since insulin caused the association between pY19-caveolin-2 and phospho-ERK as demonstrated above (Figs 3–5), we next investigated if the complex translocates together to the nucleus in response to insulin. Immunofluorescence labelling for caveolin-2, ERK, pY19-caveolin-2 and nucleus was performed after cells were treated with U0126 or wortmannin (Fig. 6). Co-localization of caveolin-2 and ERK to the nucleus was evident by insulin (Fig. 6A, *panel b*). The quantitative correlation analysis showed the expected increase in the nuclear co-localization (%) from nuclear:cytoplasmic ratios of caveolin-2 with ERK staining. Interestingly, pretreatment with U0126 prevented the insulin-induced co-localization (Fig. 6A, *panel c*). When we further examined insulin-induced translocation of pY19-caveolin-2 (Fig. 6B), insulin promoted translocation of pY19-caveolin-2 to the nucleus (Fig. 6B, *panel b*). The nuclear translocation of pY19-caveolin-2 was blocked by U0126 (Fig. 6B, *panel c*) but not affected by wortmannin treatment (Fig. 6B, *panel d*). Consistent with the results, quantitative data showed an increase in nuclear:cytoplasmic ratios of pY19-caveolin-2 staining in response to insulin.

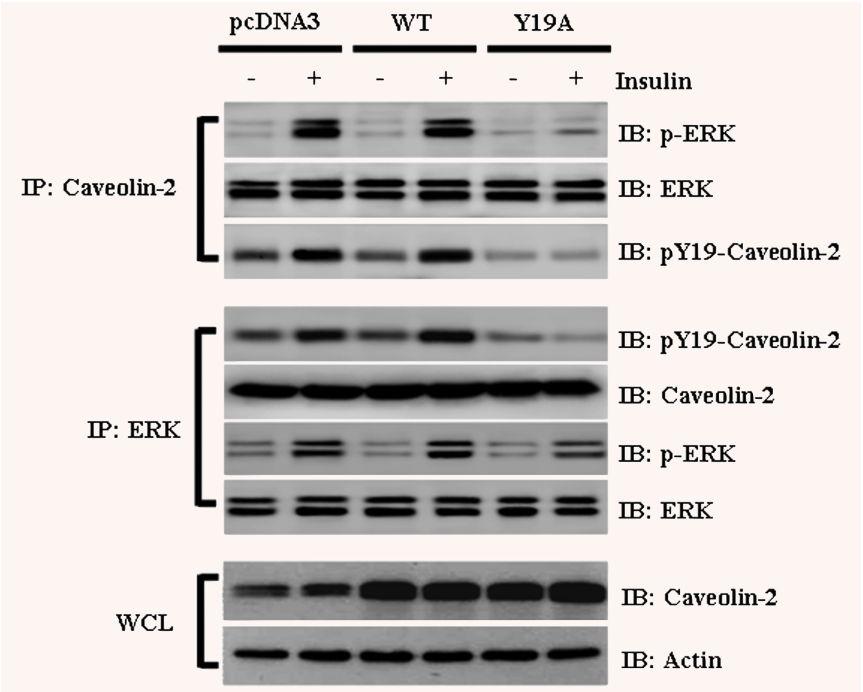

Fig. 5 Effect of transient expression of mutant caveolin-2 (Y19A) on the insulin-induced association of caveolin-2 with phospho-ERK. Hirc-B cells were transiently transfected with pcDNA3 alone (pcDNA3), pcDNA3 + caveolin-2 (WT: wild type), or pcDNA3 + caveolin-2 (Y19A: phosphorylation-deficient mutant) using the Lipofectamin transfection reagent. Thirty-six hours after transfection, the cells were lysed in 1% Triton X-100 lysis buffer B containing 0.5% Nonidet P-40 + 60 mM OG. The WCL were processed for immunoprecipitation with anti-caveolin-2 and anti-ERK antibodies and subjected to immunoblot analysis with anti-phospho-ERK, anti-ERK, anti-pY19-caveolin-2, and anti-caveolin-2 antibodies as indicated.

These immunostaining results were further confirmed by subcellular fractionation, which demonstrate that both phospho-ERK and pY19-caveolin-2 localize to nucleus in response to insulin (Fig. 6C). Consistent with the immunofluorescence microscopy findings, U0126 prevented the insulin-induced nuclear translocation of pY19-caveolin-2 with phospho-ERK but wortmannin did not affect the translocation (Fig. 6C). Our data therefore verify that insulin triggers phosphorylation of pY19-caveolin-2 and ERK in caveolin-2-ERK complex and co-localizes the complex to the nucleus.

Depletion of caveolin-2 impairs nuclear translocation of ERK by insulin without affecting ERK activation

To evaluate the role of caveolin-2 in the MAPK signalling pathway and to explore further the mechanism underlying caveolin-2-mediated ERK activation by insulin, the effects of caveolin-2 siRNA on insulin-stimulated ERK phosphorylation and nuclear translocation were examined by transfecting cells with synthetic siRNA duplexes. As shown in Fig. 7A, the caveolin-2 siRNA duplexes effectively depleted caveolin-2 protein by over 75% of levels observed in the scramble control siRNA-transfected cells. When the caveolin-2 depleted cells were examined for the activation of ERK by insulin, the knockdown of caveolin-2 had no effect on insulin-stimulated ERK activation (Fig. 7A). However, when caveolin-2 tyrosine 19 was mutated to alanine, the inhibition of insulin-induced ERK activation was observed (Fig. 5). Thus, it appears that pY19-caveolin-2 influences the activation of ERK.

Since it has been reported that activation of MAPK is required for its nuclear translocation [7, 12, 13], we next investigated the effect of caveolin-2 siRNA on translocation of the activated ERK by insulin to nucleus by immunofluorescence analysis (Fig. 7B). Consistent with the result shown in Fig. 6, the inhibition of insulin-induced nuclear translocation of ERK by U0126 was observed in the scramble control cells (Fig. 7B, *panels b and c*). However, in caveolin-2 siRNA transfected cells (Fig. 7C), insulin-induced nuclear translocation of ERK was inhibited (Fig. 7C, *panel b*). As observed in Fig. 7B, *panel c*, the same prevention of nuclear translocation of ERK by U0126 was observed in caveolin-2 siRNA transfected cells (Fig. 7C, *panel c*). Quantitative data showed a decrease in nuclear:cytoplasmic ratios of ERK staining by insulin in the caveolin-2 depleted cells. Thus, these results demonstrate that the insulin-stimulated ERK re-localization to nucleus requires caveolin-2.

siRNAs against caveolin-2 attenuate MAPK-mediated c-Jun expression and cell proliferation by insulin

To determine whether down-regulation of caveolin-2 affects the expression of c-Jun, caveolin-2 siRNA was introduced to cells. In whole cell lysates, insulin-induced 14.9-fold increase of c-Jun expression was suppressed down to a 5-fold increase by U0126 (Fig. 8A, *lanes 7 versus 9*). Knockdown of caveolin-2 caused a significant reduction from the 14.9-fold to 8.3-fold increase in the insulin-induced c-Jun expression (Fig. 8A, *lanes 3 versus 7*).

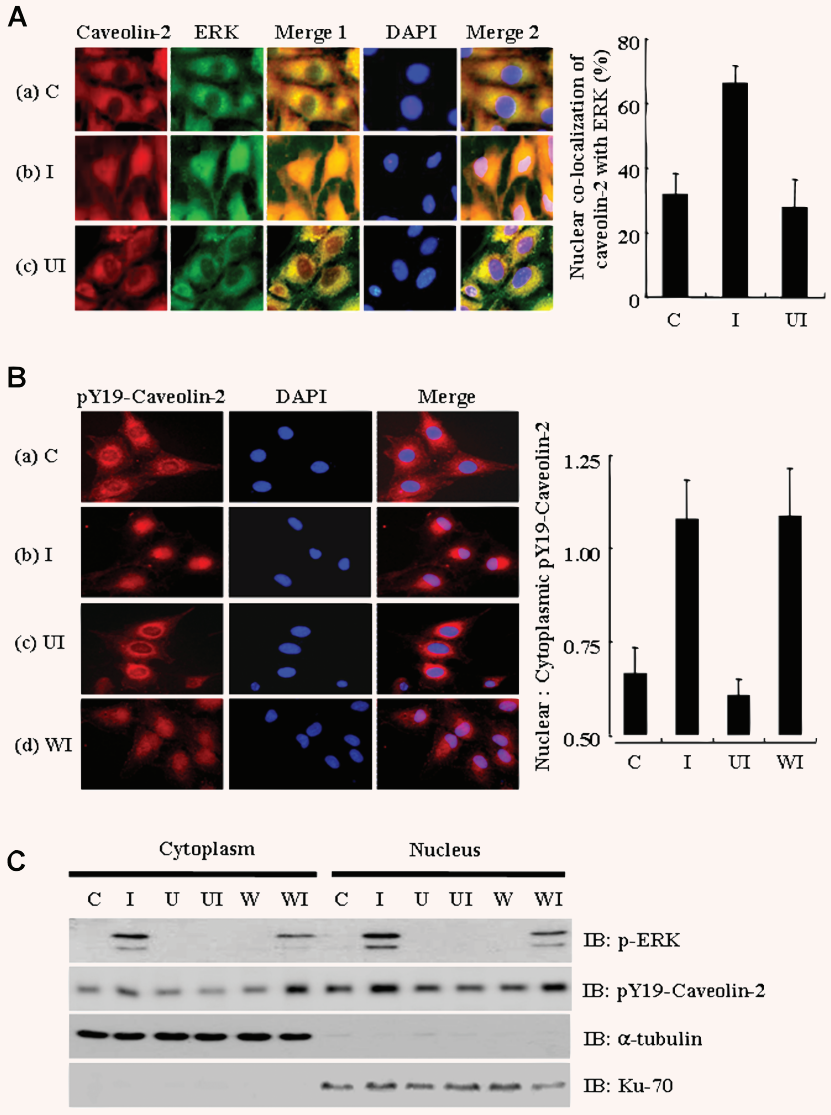

Fig. 6 Effects of U0126 and wortmannin on insulin-induced nuclear co-localization of pY19-caveolin-2 with phospho-ERK. (**A**) Confluent Hirc-B fibroblast monolayers grown on coverslips were left untreated (C); (**a**), or challenged for 10 min. with 100 nM insulin in the absence (I); (**b**) and presence of 10 μM U0126 for 2 hrs (UI); (**c**). Cells were then fixed, permeabilized and stained with anti-caveolin-2 antibody followed by TRITC-conjugated antibody, and anti-ERK antibody followed by FITC-conjugated antibody as described under 'Materials and Methods'. DNA was stained using DAPI to visualize the nucleus. Coverslips were mounted on a slide and analysed by fluorescence microscopy. *Red*: Caveolin-2, *Green*: ERK, *Blue*: Nucleus (DAPI), *Merge1*: Caveolin-2 + ERK, and *Merge2*: Caveolin-2 + ERK + DAPI. Co-localization of caveolin-2/ERK to the nucleus was quantified by ImageJ as described in 'Materials and Methods'. Percentage of nuclear co-localization from nuclear:cytoplasmic ratios of caveolin-2 with ERK staining is shown. The results represent mean ± S.E. from analysis of five separate field images of five independent experiments. A minimum of 150 cells per condition were counted. (**B**) Cells were treated as follows: (**a**), control (C); (**b**), 100 nM insulin for 10 min. (I); (**c**), 10 μM U0126 for 2 hrs plus 100 nM insulin for 10 min. (UI); (**d**), 100 nM wortmannin for 1 hr plus 100 nM insulin for 10 min. (WI). After fixation and permeabilization, cells were stained with anti-pY19-caveolin-2 antibody followed by TRITC-conjugated antibody. DNA was stained using DAPI to visualize the nucleus. *Red*: pY19-Caveolin-2, *Blue*: Nucleus (DAPI), and *Merge*: pY19-Caveolin-2 + DAPI. pY19-Caveolin-2 nuclear translocation was quantified by ImageJ. Nuclear:cytoplasmic ratios of pY19-caveolin-2 staining is shown. The results represent mean ± S.E. from analysis of three separate field images of three independent experiments. (**C**) Cells were treated with or without U0126 (10 μM) for 2 hrs or with or without wortmannin (100 nM) for 1 hr before insulin treatment (100 nM) for 10 min. and subjected to nuclear fractionation using nuclear extraction kit as described under 'Materials and Methods'. The cytoplasmic and nuclear fractions were analysed by immunoblotting using antibodies specific for phospho-ERK, pY19-caveolin-2, α-tubulin, and ku-70.

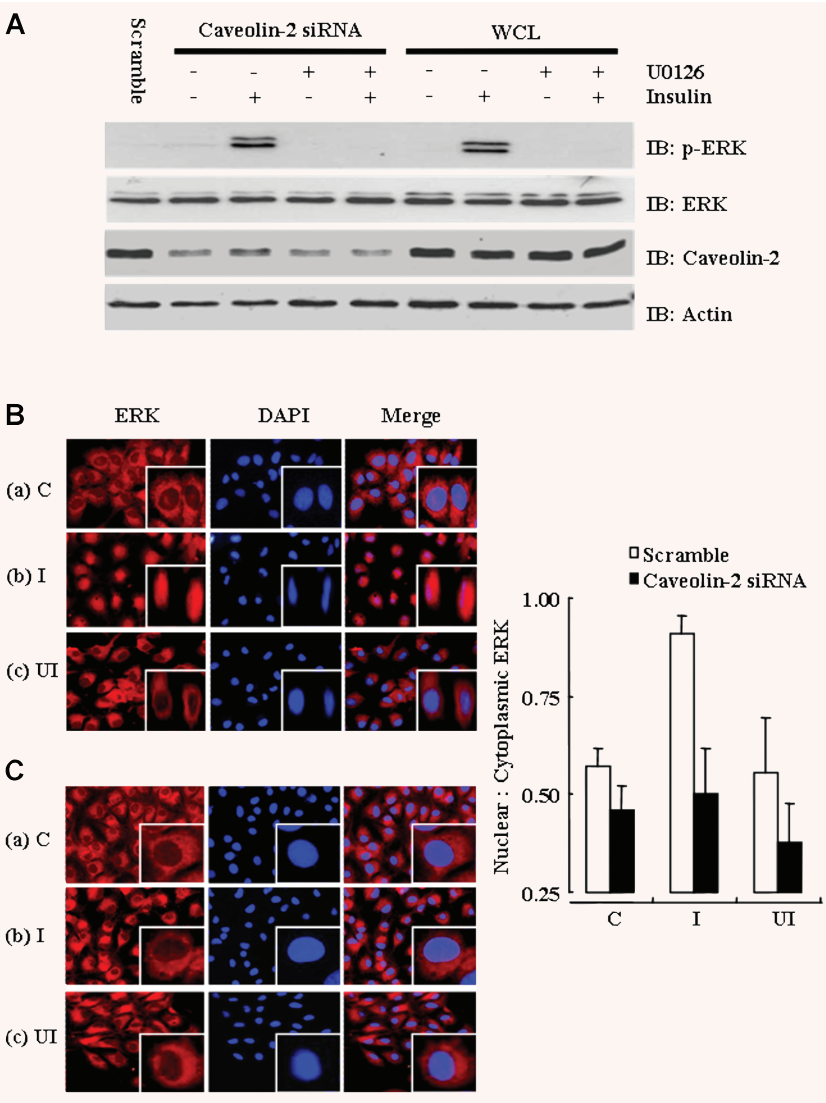

Fig. 7 Effect of caveolin-2 siRNA on insulin-stimulated phosphorylation and nuclear translocation of ERK. (**A**) For the WCL, Hirc-B cells were pretreated with or without 10 μM U0126 for 2 hrs before 100 nM insulin stimulation for 10 min. For scramble control or caveolin-2 siRNAs, cells were transfected for 48 hrs. Cells were then pretreated with or without 10 μM U0126 for 2 hrs before 100 nM insulin stimulation for 10 min. Lysates were subjected to immunoblotting using antibodies specific for phospho-ERK, ERK, caveolin-2, and actin. After transfecting cells with the scramble; (**B**) or caveolin-2 siRNAs; (**C**) for 48 hrs, cells were treated as follows: (**a**) control (C); (**b**) 100 nM insulin for 10 min. (I); (**c**) 10 μM U0126 for 2 hrs plus 100 nM insulin for 10 min. (UI). After fixation and permeabilization, cells were stained with anti-ERK antibody followed by TRITC-conjugated antibody as described under 'Materials and Methods'. To visualize nucleus DNA was stained using DAPI. Coverslips were mounted on a slide and analysed by fluorescence microscopy. *Red*: ERK, *Blue*: Nucleus (DAPI), *Merge*: ERK + DAPI. ERK nuclear translocation was quantified by ImageJ. Nuclear:cytoplasmic ratios of ERK staining is shown. The results represent mean ± S.E. from analysis of five separate field images of five independent experiments.

Importantly, cells depleted of caveolin-2 and further treated with U0126 (Fig. 8A, *lane 5*) exhibited a complete inhibition in the c-Jun expression compared to the 5-fold increase observed by U0126 alone (Fig. 8A, *lane 9*). These results reveal that caveolin-2 is involved in the MAPK-mediated c-Jun expression in response to insulin. Collectively, these data demonstrate that caveolin-2 down-regulation prevents the nuclear targeting of ERK and in turn leads to a reduction of c-Jun expression in response to insulin.

To ascertain whether insulin-triggered cell proliferation can be influenced by caveolin-2 in MAPK signalling, the effect of caveolin-2 depletion on the entry of cells into S phase was investigated. Cell proliferation was determined by counting the number of viable cells and BrdU labelling following insulin treatment. When cells were treated with both U0126 and insulin, U0126 caused an almost 40% reduction from the initial insulin-stimulated 60.6% incorporation of BrdU (data not shown). Remarkably, caveolin-2 siRNA transfection resulted in a significant decrease (42%) in BrdU labelling as compared to the scramble control with 70% increase in response to insulin (Fig. 8B). Thus, these data demonstrate that insulin-induced BrdU incorporation is regulated by caveolin-2 in cell proliferation.

Depletion of caveolin-2 attenuates MAPK-mediated cell cycle progression by insulin

To gain insight into the signalling events that link caveolin-2-mediated ERK activation to the cell cycle regulatory machinery, we investigated the involvement of caveolin-2 in ERK-mediated signalling of G1 cyclinD1 expression. To verify that cyclinD1 expression was

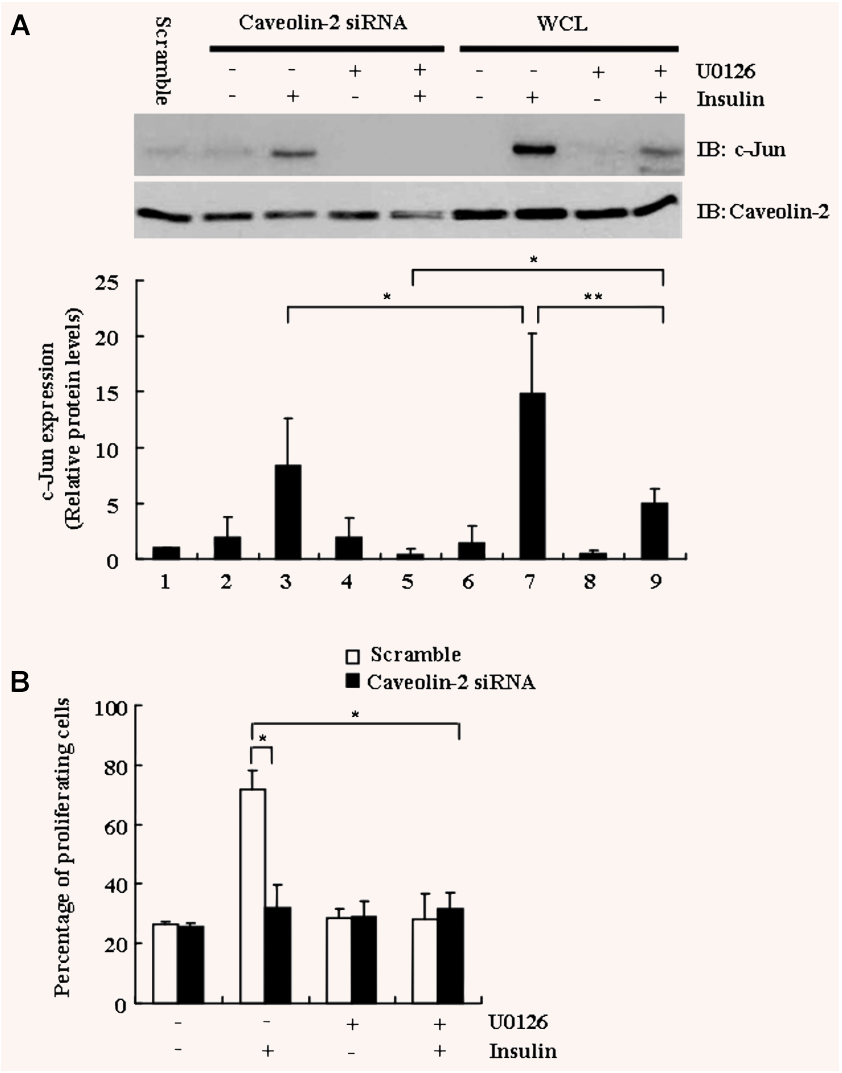

Fig. 8 Effect of caveolin-2 siRNA on insulin-induced MAPK-mediated c-Jun expression and DNA synthesis. (**A**) Hirc-B cells were pretreated with or without 10 μM U0126 for 2 hrs before 100 nM insulin stimulation for 3 hrs. WCL were subjected to immunoblotting using antibodies specific for c-Jun and caveolin-2. For scramble or caveolin-2 siRNAs, cells were transfected for 48 hrs. Cells were then pretreated with or without 10 μM U0126 for 2 hrs before 100 nM insulin stimulation for 3 hrs and lysates were immunoblotted with antibodies specific to c-Jun and caveolin-2. Insulin-induced c-Jun expression was quantified by densitometry. Each bar represents mean ± S.E of five independent experiments. *, $P < 0.01$; **, $P < 0.001$. (**B**) Scramble or caveolin-2 siRNAs were transfected for 48 hrs. Cells were then treated with or without 10 μM U0126 for 2 hrs before 100 nM insulin for 10 min. treatment. DNA synthesis was determined by quantitating BrdU incorporated into the newly synthesized DNA during cell proliferation. Quantification shown was insulin-induced proliferating cells detected as compared to the control cells; mean ± S.E., $n = 3$. *, $P < 0.001$.

mediated by MAPK, cells were treated with U0126. The insulin-induced 6.2- and 6.6-fold increases in cyclinD1 mRNAs and protein levels, respectively, were inhibited by U0126 (Fig. 9, A and B, respectively). To determine whether caveolin-2 is required for the ERK-mediated cell cycle progression, caveolin-2 siRNAs were transfected. As shown in Fig. 9C, *lanes 2 versus 6*, caveolin-2-depleted cells exhibited a 2-fold reduction in the mRNA levels of cyclinD1 as compared to the scramble control in response to insulin. When caveolin-2-depleted cells were pretreated with U0126, however, the elevation in insulin-induced cyclinD1 mRNA levels of the scramble control cells was completely repressed (Fig. 9C, *lanes 4 versus 8*). Thus, these data demonstrate that caveolin-2 positively regulates ERK-mediated cell cycle progression by insulin.

It is well known that ERK indirectly controls the activity of cell cycle regulators, such as cyclins, cyclin-dependent kinases (cdks), and their inhibitors including p21 [8]. When cells were treated with U0126 to verify whether the attenuation of p21 mRNAs was mediated by MAPK, no significant change in p21 mRNAs level by U0126 was detected (Fig. 9D), indicating that p21 is not related to MAPK signalling. In addition, caveolin-2 siRNAs also did not cause any significant changes in the mRNA levels (data not shown). Thus, our data suggest that p21 is regulated independently of caveolin-2-mediated MAPK signalling pathway.

The actin cytoskeleton-dependent pathway is required for pY19-caveolin-2-mediated phospho-ERK nuclear translocation by insulin

To test whether actin cytoskeleton is involved in the insulin-induced nuclear localization of pY19-caveolin-2 with phospho-ERK, cells were treated with CCD or LatB. Application of insulin led to

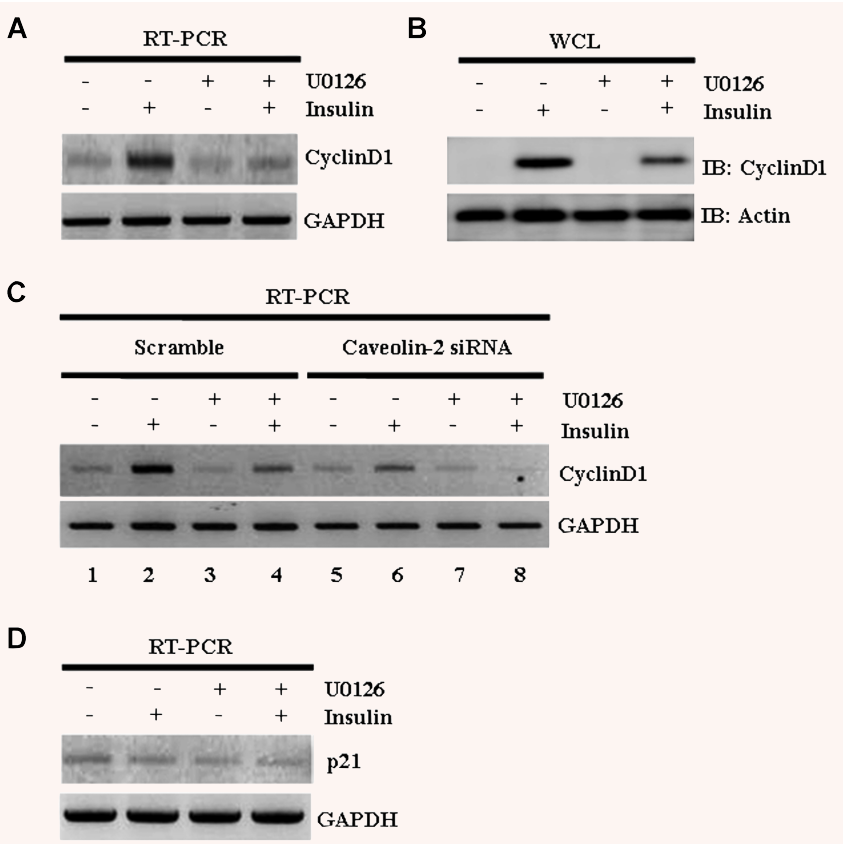

Fig. 9 Effect of caveolin-2 siRNA on MAPK-mediated cyclinD1 and p21 expression by insulin. (**A**) Hirc-B cells were pretreated with or without 10 μM U0126 for 2 hrs before 100 nM insulin stimulation for 3 hrs. CyclinD1 mRNA levels were analysed by RT-PCR as described under 'Materials and Methods'. (**B**) Protein levels of cyclinD1 were analysed by immunoblot analysis with anti-cyclinD1 antibody. (**C**) Cells were stably transfected with each of the scramble and caveolin-2 siRNAs. Cells were then pretreated with or without 10 μM U0126 for 2 hrs and treated with or without 100 nM insulin for 3 hrs. Total RNA were extracted and the amount of cyclinD1 mRNAs were analysed by the RT-PCR. (**D**) Cells were pretreated with or without 10 μM U0126 for 2 hrs before 100 nM insulin stimulation for 3 hrs. p21 mRNA levels were analysed by the RT-PCR. GAPDH was co-amplified as the internal control in (**A**), (**C**) and (**D**).

nuclear co-localization of pY19-caveolin-2 with phospho-ERK (Fig. 10A, *panel b*). Addition of CCD or LatB evidently abrogated insulin-induced nuclear co-localization of pY19-caveolin-2 with phospho-ERK (Fig. 10A, *panels d and f*). Consistent with the results, quantitative data showed decreases in the nuclear co-localization (%) from nuclear:cytoplasmic ratios of pY19-caveolin-2 with phospho-ERK stainings by disruption of the cytoskeleton in response to insulin.

To confirm the immunostaining results demonstrating that the actin cytoskeleton participates in the nuclear translocation of ERK and caveolin-2, we performed subcellular fractionation. As shown in Fig. 10B, CCD and LatB markedly prevented insulin-induced nuclear localization of pY19-caveolin-2. The inhibition of phospho-ERK nuclear localization by CCD and LatB was also observed. Analysis of the subcellular localization showed that insulin increased nuclear accumulation of phospho-ERK by 56%. In contrast, phospho-ERK was predominantly localized in cytoplasm (63–65%) in CCD- and LatB-treated cells. Collectively, our data demonstrate that the insulin-elicited pY19-caveolin-2-mediated translocation of phospho-ERK from the cytoplasm to the nucleus depends on the intact cellular actin cytoskeleton.

Discussion

In this report, we have presented data that suggest a novel role for pY19-caveolin-2 as a key mediator for ERK activation and translocation to the nucleus in insulin signalling. Although we previously showed that caveolin-2 can associate with ERK [33], our report herein is the first to document that pY19-caveolin-2 positively regulates ERK signalling in response to insulin and participates directly in the regulation of mitogenic insulin signalling. We show that incubation of cells with insulin induced: (*i*) tyrosine phosphorylation of caveolin-2; (*ii*) association between pY19-caveolin-2 with phospho-ERK; (*iii*) nuclear re-localization of pY19-caveolin-2 with phospho-ERK; (*iv*) expression of c-Jun; (*v*) DNA synthesis and (*vi*) expression of cyclinD1. In addition, we demonstrate that the mitogenic effect of insulin is mediated by pY19-caveolin-2 *via* actin cytoskeleton-dependent MAPK signalling pathway.

Our investigation for the functional role of the insulin-induced tyrosine phosphorylation of caveolin-2 reveals that pY19-caveolin-2 displays its distinctive interaction with signalling molecules in insulin signalling cascade. In order to define the regulatory mechanism by pY19-caveolin-2 involved in the insulin signalling

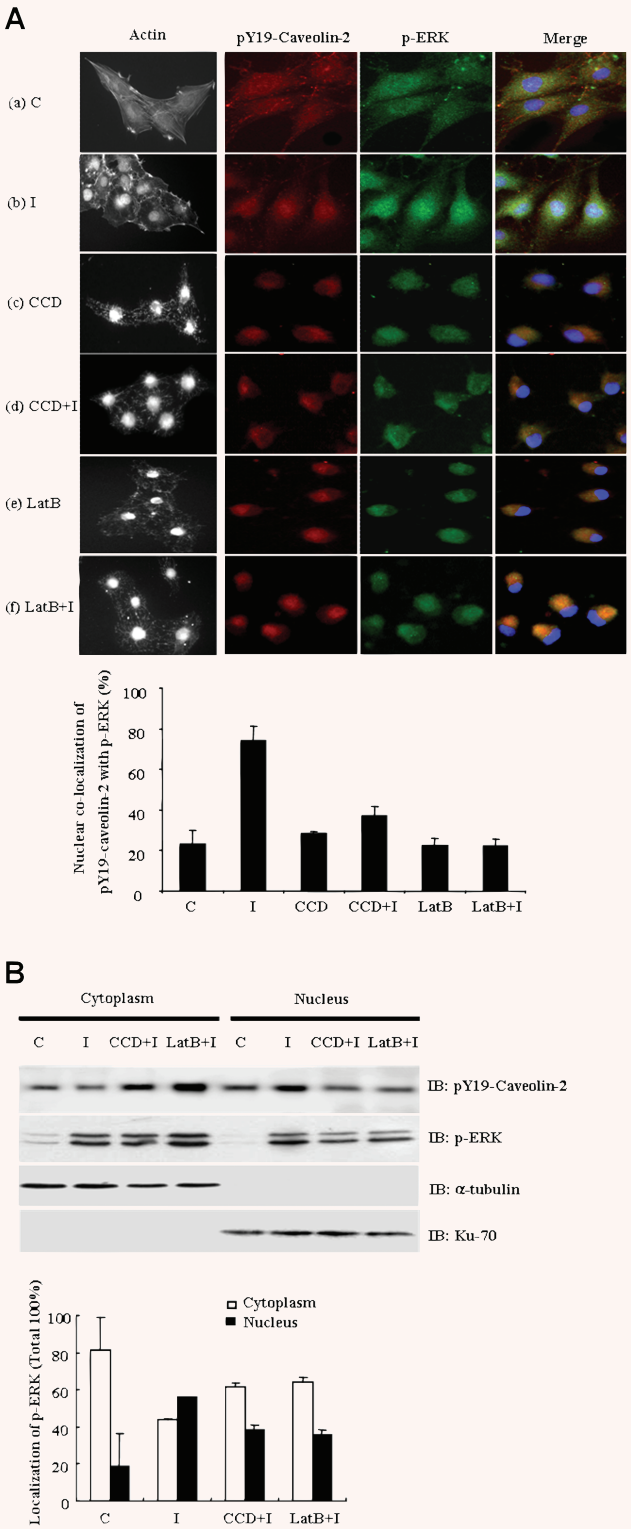

Fig. 10 Effect of cytochalasin-D and latrunculin B on insulin-induced nuclear co-localization of pY19-caveolin-2 with phospho-ERK. Confluent Hirc-B cells grown on coverslips were left untreated (C) (**a**), challenged with 100 nM insulin for 10 min. (I) (**b**), treated with 1 μM CCD for 15 min. alone (CCD) (**c**), pre-treated with 1 μM CCD for 15 min. before 100 nM insulin stimulation for 10 min. (CCD+I) (**d**), treated with 1 μM LatB for 30 min. alone (LatB) (**e**), pre-treated with 1 μM LatB for 30 min. before 100 nM insulin stimulation for 10 min. (LatB+I) (**f**). Cells were then fixed, permeabilized and stained with anti-F-actin, anti-pY19-caveolin-2 and anti-phospho-ERK antibodies followed by TRITC- or Alexa Fluor® 488-conjugated antibodies as described under 'Materials and Methods'. DNA was stained using DAPI to visualize the nucleus and F-actin using FITC-conjugated phalloidin. Coverslips were mounted on a slide and analysed by fluorescence microscopy. *Gray*: F-actin, *Red*: pY19-caveolin-2, *Green*: phospho-ERK, *Merge*: pY19-caveolin-2 + phospho-ERK + nucleus (DAPI). Co-localization of pY19-caveolin-2 with phospho-ERK to the nucleus was quantified by ImageJ. Percentage of nuclear co-localization from nuclear:cytoplasmic ratios of pY19-caveolin-2 with phospho-ERK staining is shown. The results represent mean ± S.E. from analysis of five separate field images of three independent experiments. (**C**) Hirc-B cells were treated with CCD (1 μM) for 15 min. or LatB (1 μM) for 30 min. before insulin treatment (100 nM) for 10 min. and subjected to nuclear fractionation using nuclear extraction kit as described under 'Materials and Methods'. The cytoplasmic and nuclear fractions were analysed by immunoblotting using antibodies specific for phospho-ERK, pY19-caveolin-2, α-tubulin, and ku-70. Quantification shown represents the relative levels of phospho-ERK cellular distribution (%) in cytoplasm and nucleus detected as compared to the control sample; mean ± S.E., $n = 3$.

pathway, effects of the specific inhibitors U0126 and wortmannin of the MAPK and PI3K pathways, respectively, were examined. Our data show that U0126 specifically reduces the insulin-induced phosphorylation of pY19-caveolin-2 and inhibits its interaction with phospho-ERK. However, the insulin-induced pY19-caveolin-2 and association with phospho-ERK was not changed by wortmannin. The present results provide the first evidence that pY19-caveolin-2 specifically associates with phospho-ERK in response to insulin. Furthermore, phosphorylation of caveolin-2 at tyrosine 19 is required for the activation of ERK and before insulin-induced interaction of caveolin-2 with phospho-ERK. Thus, our findings indicate that the insulin-induced association of pY19-caveolin-2 and phospho-ERK is mediated by pY19-caveolin-2 to regulate down stream mitogenic signalling by insulin. The interaction is confirmed in various cell types and has characterized a novel signalling pathway with mechanistic insights with the functional significance.

When we explored the role of caveolin-2 in the insulin-elicited nuclear translocation of ERK by applying caveolin-2 siRNA, down-regulation of caveolin-2 by siRNA inhibits insulin-induced nuclear translocation of ERK with no changes in ERK activation by insulin. Thus, the present findings demonstrate that caveolin-2 is required for insulin-elicited translocation of ERK to nucleus and strongly support that caveolin-2 acts as a key regulator for cellular localization of ERK by insulin. The importance of caveolin-2 is further supported by the finding that depleted caveolin-2 by siRNA reduced the c-Jun expression in response to insulin. In addition, when caveolin-2 depleted cells were treated with U0126, insulin-induced c-Jun expression was completely inhibited. Our results also show that insulin-stimulated DNA synthesis requires ERK activation and ERK translocation to the nucleus with the assistance of caveolin-2. Thus, our data collectively demonstrate that the inhibition of ERK nuclear translocation by caveolin-2 siRNA results in the attenuation of insulin-induced c-Jun expression and DNA synthesis by ERK and point out that caveolin-2 has a critical regulatory role in ERK translocation to the nucleus.

As cyclinD1 expression is generally regulated by the MAPK signalling pathway [6, 40], our results show that the insulin-stimulated ERK activation is linked to the increase in mRNA and protein levels of cyclinD1. However, the insulin-stimulated increase of cyclinD1 mRNAs was completely inhibited when caveolin-2 depleted cells were treated with U0126. p21 is known to induce growth arrest and to possess apoptotic functions [41]. Insulin-induced reduction of p21 mRNAs coincided with the highest induction of cyclinD1 mRNA at 3 hrs of incubation (data not shown). However, insulin-induced p21 mRNA induction exhibited no remarkable changes upon U0126 treatment and caveolin-2 siRNA transfection (data not shown) in contrast to the reduction in cyclinD1 mRNA levels. Thus, it would appear that caveolin-2-mediated mitogenic insulin signalling for cell proliferation and growth is not linked to p21-regulated apoptosis pathway. Thus, the results suggest that caveolin-2 in parallel with ERK activation regulates the insulin-induced G1 phase progression of cell-cycle. Importantly, our data show that depletion of caveolin-2 results in a significant retardation of mitogenic insulin signalling, which is correlated with the failure in the translocation of ERK to the nucleus. This impairment has a consequent inhibitory effect on the down stream cascade of the insulin action. Thus, it is apparent that the insulin-induced c-Jun expression and DNA synthesis, and the subsequent activation of the G0/G1 to S phase transition of the cell cycle by cyclinD1 are achieved concomitantly with an increase in the phosphorylation of caveolin-2 and ERK, the interaction between pY19-caveolin-2 and phospho-ERK, and more importantly the nuclear translocation of that complex.

Insulin causes a rapid remodelling of actin filaments, promoting membrane ruffling in various cells [42, 43]. CCD and LatB, actin depolymerizing agents prevented stretch-induced ERK activation and nuclear translocation in cardiomyocytes and vascular smooth muscle cells [44, 45]. However, CCD and LatB failed to influence ERK phosphorylation or translocation of ERK to the nucleus in smooth muscle cell mitogenesis caused by serotonin [46]. Our data show that disassembly of the actin network by CCD and LatB impaired the insulin-induced nuclear co-localization of pY19-caveolin-2 with phospho-ERK. Thus, our data demonstrate that insulin-stimulated actin remodelling is required for insulin-induced association of pY19-caveolin-2 with phospho-ERK and nuclear co-localization of pY19-caveolin-2 with phospho-ERK. These findings provide a mechanism whereby insulin exerts actin cytoskeleton-dependent association of pY19-caveolin-2 with phospho-ERK and their nuclear re-localization.

In summary, the present study provides evidence for a caveolin-2-mediated actin cytoskeleton-dependent mechanism that is activated by insulin to regulate MAPK signalling. Insulin triggers phosphorylation of caveolin-2 at tyrosine 19. pY19-Caveolin-2 specifically interacts with phospho-ERK. The interaction leads to the translocation of phospho-ERK from the cytoplasm to the nucleus that depends on an intact actin cytoskeleton. Once activated ERK enters the nucleus, phospho-ERK regulates nuclear proteins including transcription factors to enhance the mitogenic signalling of insulin. These transcription factors, finally, regulate expression of diverse genes related to control the proliferation and growth of cells. Thus, pY19-caveolin-2 could regulate cell fate by acting as a mediator molecule linking the ERK signalling cascade with the spatial coordination regulated by cross-talk among actin, caveolin-2 and ERK in response to insulin.

Evidence of the role of caveolin in cancer cells has been well documented, wherein specifically caveolin-1 is down-regulated in transformed cells and has a tumor suppressor activity [22–26]. Senescent cells exhibited elevated levels of caveolin-1 and the morphologies of senescent cells became young cell-like by down-regulation of caveolin-1 [27–29]. Thus, it is apparent that caveolin-1 plays a negative role in the regulation of both aging and cancer. On the contrary, our results demonstrate that caveolin-2, widely presented in normal, senescent and tumor cells [17–21, 27–30], positively regulates cell growth and proliferation. These results imply that normal cell proliferation and growth might be controlled by homeostasis of caveolin-1 and

caveolin-2 status. Therefore, our findings identify caveolin-2 as an important positive regulator of cellular mitogenesis of the MAPK pathway and a potential target for the treatment of cancers and aging. Furthermore, the present functional characterization of caveolin-2 could also provide new insights into the understanding both insulin and growth factor signalling in mammalian cells.

Acknowledgements

This work was supported in part by the fund of Research Promotion Program (RPP-2006-020), Gyeongsang National University and by a grant from the MOST/KOSEF to the EBNCRC to YP. HK and KJ were supported by scholarships from the BK21 Program, the Ministry of Education and Human Resources Development, Korea.

References

1. **Saltiel AR, Pessin JE.** Insulin signaling pathways in time and space. *Trends Cell Biol*. 2002; 12: 65–71.
2. **Saltiel AR**, **Kahn CR.** Insulin signalling and the regulation of glucose and lipid metabolism. *Nature*. 2001; 414: 799–806.
3. **Le Roith D, Zick Y.** Recent advances in our understanding of insulin action and insulin resistance. *Diabetes Care*. 2001; 24: 588–97.
4. **Schaeffer HJ, Weber MJ.** Mitogen-activated protein kinases: specific messages from ubiquitous messengers. *Mol Cell Biol*. 1999; 19: 2435–44.
5. **Robinson MJ**, **Cobb MH.** Mitogen-activated protein kinase pathways. *Curr Opin Cell Biol*. 1997; 9: 180–6.
6. **Lavoie JN, L'Allemain G, Brunet A, *et al.*** Cyclin D1 expression is regulated positively by the p42/p44MAPK and negatively by the p38/HOG MAPK pathway. *J Biol Chem*. 1996; 271: 20608–16.
7. **Brunet A, Roux D, Lenormand P, *et al.*** Nuclear translocation of p42/p44 mitogen-activated protein kinase is required for growth factor-induced gene expression and cell cycle entry. *EMBO J*. 1999; 18: 664–74.
8. **Wilkinson MG, Millar JBA.** Control of the eukaryotic cell cycle by MAP kinase signalling pathways. *FASEB J*. 2000; 14: 2147–57.
9. **Pearson G, Robinson F, Beers Gibson T, *et al.*** Mitogen-activated protein (MAP) kinase pathways: regulation and physiological functions. *Endocr Rev*. 2001; 22: 153–83.
10. **Yoon S, Seger R.** The extracellular signal-regulated kinase multiple substrates regulate diverse cellular functions. *Growth Factors*. 2006; 24: 21–44.
11. **Whitmarsh AJ, Davis RJ.** A central control for cell growth. *Nature*. 2000; 403: 255–6.
12. **Lenormand P, Brondello JM, Brunet A, Pouysségur J.** Growth factor-induced p42/p44 MAPK nuclear translocation and retention requires both MAPK activation and. neosynthesis of nuclear anchoring proteins. *J Cell Biol*. 1998; 142: 625–33.
13. **Khokhlatchev AV, Canagarajah B, Wilsbacher J, *et al.*** Phosphorylation of the MAP kinase ERK2 promotes its homodimerization and nuclear translocation. *Cell*. 1998; 93: 605–15.
14. **Ebisuya M, Kondoh K, Nishida E.** The duration, magnitude and compartmentalization of ERK MAP kinase activity: mechanisms for providing signaling specificity. *J Cell Sci*. 2005; 118: 2997–3002.
15. **Murphy LO, MacKeigan JP, Blenis J.** A network of immediate early gene products propagates subtle differences in mitogen-activated protein kinase signal amplitude and duration. *Mol Cell Biol*. 2004; 24: 144–53.
16. **Minshull J, Sun H, Tonks NK, Murray AW.** A MAP kinase-dependent spindle assembly checkpoint in Xenopus egg extracts. *Cell*. 1994; 79: 475–86.
17. **Cohen AW, Combs TP, Scherer PE, Lisanti MP.** Role of caveolin and caveolae in insulin signaling and diabetes. *Am J Physiol Endocrinol Metab*. 2003; 285: E1151–60.
18. **Gratton JP, Bernatchez P, Sessa WC.** Caveolae and caveolins in the cardiovascular system. *Circ Res*. 2004; 94: 1408–17.
19. **Scherer PE, Lewis RY, Volonte D, *et al.*** Cell-type and tissue-specific expression of caveolin-2. *J Biol Chem*. 1997; 272: 29337–46.
20. **Razani B, Woodman SE, Lisanti MP.** Caveolae: from cell biology to animal physiology. *Pharmacol Rev*. 2002; 54: 431–67.
21. **Liu P, Rudick M, Anderson RGW.** Multiple functions of caveolin-1. *J Biol Chem*. 2002; 277: 41295–8.
22. **Engelman JA, Lee RJ, Karnezis A, *et al.*** Reciprocal regulation of neu tyrosine kinase activity and caveolin-1 protein expression *in vitro* and *in vivo*: implications for human breast cancer. *J Biol Chem*. 1998; 271: 6518–22.
23. **Lee SW, Reimer CL, Oh P, *et al.*** Tumor cell growth inhibition by caveolin re-expression in human breast cancer cells. *Oncogene*. 1998; 16: 1391–7.
24. **Hulit J, Bash T, Fu M, *et al.*** The cyclin D1 gene is transcriptionally repressed by caveolin-1. *J Biol Chem*. 2000; 275: 21203–9.
25. **Engelman JA, Chu C, Lin A, *et al.*** Caveolin-mediated regulation of signaling along the p42/44 MAP kinase cascade *in vivo*. A role for the caveolin-scaffolding domain. *FEBS Lett*. 1998; 428: 205–11.
26. **Galbiati F, Volonté D, Engelman JA, *et al.*** Targeted down-regulation of caveolin-1 is sufficient to drive cell transformation and hyperactivate the p42/44 MAP kinase cascade. *EMBO J*. 1998; 17: 6633–48.
27. **Cho KA, Ryu SJ, Park JS, *et al.*** Senescent phenotype can be reversed by reduction of caveolin status. *J Biol Chem*. 2003; 278: 27789–95.
28. **Cho KA, Ryu SJ, Oh YS, *et al.*** Morphological adjustment of senescent cells by modulating caveolin-1 status. *J Biol Chem*. 2004; 279: 42270–8.
29. **Volonte D, Zhang K, Lisanti MP, Galbiati F.** Expression of caveolin-1 induces premature cellular senescence in primary cultures of murine fibroblasts. *Mol Biol Cell*. 2002; 13: 2502–17.
30. **Scherer PE, Okamoto T, Chun M, *et al.*** Identification, sequence and expression of caveolin-2 defines a caveolin gene family. *Proc Natl Acad Sci USA*. 1996; 93: 131–5.
31. **Lee H, Park DS, Wang XB, *et al.*** Src-induced phosphorylation of caveolin-2 on tyrosine 19. *J Biol Chem*. 2002; 277: 34556–67.
32. **Wang XB, Lee H, Capozza F, *et al.*** Tyrosine phosphorylation of caveolin-2 at residue 27: differences in the spatial and temporal behavior of phospho-cav-2 (pY19 and pY27). *Biochemistry*. 2004; 43: 13694–706.
33. **Sowa G, Pypaert M, Fulton D, Sessa WC.** The phosphorylation of caveolin-2 on

serines 23 and 36 modulates caveolin-1-dependent caveolae formation. *Proc Natl Acad Sci USA*. 2003; 100: 6511–6.

34. **Razani B, Wang XB, Engelman JA, *et al.*** Caveolin-2-deficient mice show evidence of severe pulmonary dysfunction without disruption of caveolae. *Mol Cell Biol*. 2002; 22: 2329–44.
35. **Kim S, Pak Y.** Caveolin-2 regulation of the cell cycle in response to insulin in Hirc-B fibroblast cells. *Biochem Biophys Res Comm*. 2005; 330: 88–96.
36. **Head BP, Patel HH, Roth DM, *et al.*** Microtubules and actin microfilaments regulate lipid raft/caveolae localization of adenylyl cyclase signaling components. *J Biol Chem*. 2006; 281: 26391–9.
37. **Lockwich TP, Liu X, Singh BB, *et al.*** Assembly of Trp1 in a signaling complex associated with caveolin-scaffolding lipid raft domains. *J Biol Chem*. 2000; 275: 11934–42.
38. **Novitskaya V, Makarava N, Bellon A, *et al.*** Probing the conformation of the prion protein within a single amyloid fibril using a novel immunoconformational assay. *J Biol Chem*. 2006; 281: 15536–45.
39. **Noursadeghi M, Tsang J, Haustein T, *et al.*** Quantitative imaging assay for NF-κB nuclear translocation in primary human macrophages. *J Immunol Methods*. 2008; 329: 194–200.
40. **Cheng M**, **Sexl V**, **Sherr CJ**, **Roussel MF.** Assembly of cyclin D-dependent kinase and titration of p27/KIP1 regulated by mitogen-activated protein kinase kinase (MEK1). *Proc Natl Acad Sci USA*. 1998; 95: 1091–6.
41. **Evan GI, Vousden KH.** Proliferation, cell cycle and apoptosis in cancer. *Nature*. 2001; 411: 342–8.
42. **Clodi M, Vollenweider P, Klarlund J, *et al.*** Effects of general receptor for phosphoinositides on insulin and insulin-like growth factor I-induced cytoskeletal rearrangement, GLUT4 translocation, and deoxyribonucleic acid synthesis. *Endocrinology*. 1998; 139: 4984–90.
43. **Wang QH, Bilan PJ, Tsakiridis T, *et al.*** Actin filaments participate in the relocalization of phosphatidylinositol 3-kinase to glucose transporter-containing compartments and in the stimulation of glucose uptake in 3T3-L1 adipocytes. *Biochem J*. 1998; 331: 917–28.
44. **Kawamura S**, **Miyamoto S**, **Brown JH.** Initiation and transduction of stretch induced Rho and Rac1 activation through caveolae. *J Biol Chem*. 2003; 278: 31111–7.
45. **Numaguchi K, Eguchi S, Yamakawa T, *et al.*** Mechanotrans-duction of rat aortic vascular smooth muscle cells requires RhoA and intact actin filaments. *Circ Res*. 1999; 85: 5–11.
46. **Liu Y, Suzuki YJ, Day RM, Fanburg BL.** Rho kinase-induced nuclear translocation of ERK1/2 in smooth muscle cell mitogenesis caused by serotonin. *Circ Res*. 2004; 95: 579–86.